University of Bath

Alternative formats
If you require this document in an alternative format, please contact:
openaccess@bath.ac.uk

Multifunctional Reduced Graphene Oxide Coating on Laminated Composites

Mario Rapisarda[a1], Michele Meo[a]

[a]Department of Mechanical Engineering, University of Bath, Bath, BA2 7AY, UK

Abstract

Carbon Fibre Reinforced Plastics (CFRPs) are commonly used for structural applications due to their high specific mechanical properties. CFRPs can also be functionalized exploiting a combination of several materials that introduce multifunctional features to the global performance of a structure and widen their range of operations. This work investigates the use of a Reduced Graphene Oxide (RGO) Film as multifunctional coating on CFRP laminates. Exploiting the inherent properties of these films, surface properties of composite structures such as electrical conductivity and wettability can be improved. Moreover, potential built-in functions, as live strain sensing and DC-biased thermography, are studied. Three point bending tests demonstrated a negligible influence of the RGO films on the flexural properties of the CFRP laminates and confirmed a satisfying adhesion between the coating and the structure.

Keywords: Electrical Conductivity, Thermography, Hydrophobicity, Multifunctional Composite Structures, Reduced Graphene Oxide (RGO) Films.

1. Introduction

Carbon, in nature, can be found in two allotropes: diamond and graphite. Both are characterized by a well ordered three-dimensional (3D) structure consisting in extended networks of sp^3 and sp^2 hybridized carbon atoms, respectively [1]. In the last two decades, other synthetic carbon allotropes, all based on sp^2 hybridized carbon atoms with different spatial arrangements, were discovered: zero-dimensional (0D) Fullerene in 1985 [2], one-dimensional (1D) Carbon nanotubes in 1991 [3] and two-dimensional (2D) Graphene in 2004 [4]. In particular, the 2D graphene can be considered as the basic building block of 0D fullerenes, 1D carbon nanotubes and 3D graphite [4, 5]

Single-layer graphene, thanks to its atomic structure, is characterised by an extremely high thermal conductivity, $\approx$3,000 W mK^{-1} [6], high mobility of charge carriers, $\approx$2000,000 cm^2 V^{-1} s^{-1} [7] and hydrophobicity [8]. However, its production for technological applications is still a major challenge and other routes to exploit its outstanding properties must be considered. Reduced Graphene Oxide (RGO), a compound made of mono or few layers of graphene having oxygen functionalities on its basal planes and edges [9], is nowadays one of the main candidate for the high scale production of graphene based materials. Thanks to chemical, thermal or mechanical functionalisation, products having applications such as water treatment, energy storage, and plastic composite reinforcements, among others, can be fabricated [10-13]. Particularly, RGO can be manufactured in light-weight thin films having densities of 1.9 g cm^{-3}. Even if they show a decrease of the overall performances with respect of pristine single-layer graphene, due to the stacking of many layers and the existence of impurities [14, 15], they can still be considered as interesting candidate to functionalise composite plastics like Carbon Fibre Reinforced Polymers (CFRPs).

The latter consists in a polymeric resin, called matrix, with carbon fibres as reinforcement [16]. Due to their structure, CFRPs show high specific mechanical properties, such as stiffness and strength, and so they are commonly used for structural applications in many different fields, from the civil [17] to the aerospace industries [18]. In order to improve their range of applications, CFRPs may be combined with materials having specialized properties aiming to introduce unique features to the global performances of a structure. The manufacturing of multifunctional CFRPs can be obtained embedding an array of metal reinforcements to improve the mechanical properties and provide both Structural Health Monitoring (SHM) and de-icing functionalities [19]. Another solution is the use of special designs to develop antenna/sensor systems, obtaining the capability to perform SHM wirelessly [20]. Furthermore, the

---

* Corresponding author. Tel.: +44 7711949584.
E-mail address: m.rapisarda@bath.ac.uk

embedding of graphite film or thin solid state batteries can, respectively, improve the through thickness thermal conductivity [21] or introduce energy storage abilities [22].

The aim of this work is to introduce a novel approach in developing multifunctional composite structures, using light-weight RGO films as superficial coating on CFRP laminates in a single cycle manufacturing process. First, the RGO film was analysed with X-Ray Diffractometry (XRD) and Raman Spectroscopy to characterize its chemical-physical structure. Then surface properties such as electrical resistance and wettability of the composite were investigated. The mechanical characterisation and a preliminary adhesion evaluation were performed via three point bending tests. Ultimately, newly enabled functionalities, namely live strain-sensing and Direct Current (DC)-biased thermography, and their effectiveness were explored.

2. Experimental

2.1. Materials and Methods

The RGO Films were produced as follows. A Graphite Oxide (GtO), that was purchased in powdered form from XIAMEN TOB NEW ENERGY TECHNOLOGY Co., LTD, dispersion in distilled water was exfoliated to GO using a probe sonicator (Dr. Hielscher GmbH UP100H) in ice bath and then casted on a Polyethylene Terephthalate (PET) film. After 24 h of drying in ambient condition, a GO Film was obtained. The latter was finally annealed at a temperature of 1300 °C for 3h under Ar gas atmosphere and calendered to obtain the RGO Films with a thickness of 40 µm.

The multifunctional RGO/CFRP composite laminate was manufactured in a single cycle process of lamination and autoclave moulding. A unidirectional carbon fibre reinforced prepreg (CYCOM® 977-2) was laminated to obtain a 3 plies symmetric laminate with a [90-0-90] stacking sequence. Afterwards, the 40 µm thick RGO film was directly laminated on top of the uncured laminate. A representative scheme is reported in Fig. 1. A traditional CFRP laminate with no RGO coating was manufactured as reference. Both laminates (RGO/CFRP and traditional CFRP) were then cured in autoclave using a cycle of 3 h at 180 °C and 100 psi. The cured laminates were then cut to specific sizes for the experimental campaign using a diamond blade saw.
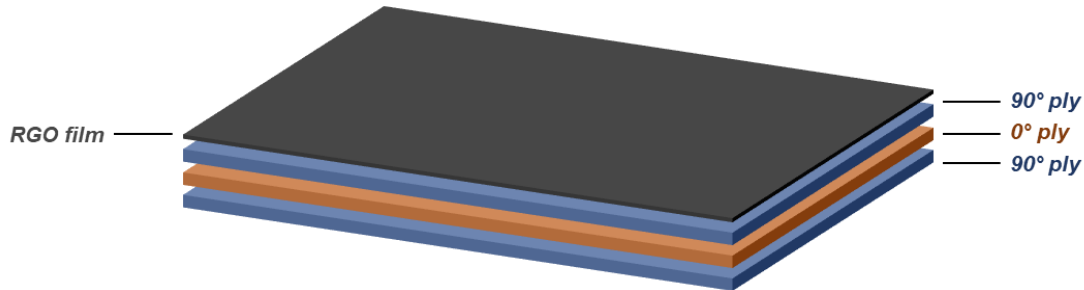

Fig. 1. Representative scheme of the multifunctional RGO/CFRP composite laminate.

2.2. Characterization

X-Ray Diffractometry was performed in a range of 2θ = 4 – 50 ° at room temperature using a STOE STADI P diffractometer (Cu-Kα generator, 1.54 Å, 40 kV, 40 mA) in transmission mode for crystalline phases identification. The Raman spectrum was obtained with a Renishaw inVia Raman Microscope with an IK Series He-Cd 523 nm laser and analysed with the proprietary software WiRe for number and quality of graphene layers monitoring.

A Jandel Multiheigh Four Point Probe Station coupled with a Keysight 34465A digital multimeter was used to measure the electrical properties of the surface of the samples. The Sheet Resistance or Surface Resistivity (R_s) is an electrical property used to characterize the ability of the current to flow through a thin film, considering the electrodes at the opposite sides of a square of any size. Due to the latter, although the physical unit is Ohms (Ω), in practice the value is often given in Ohms per Square (Ω sq^{-1}). This allows the distinction with the Electrical Resistance (R) whose unit is Ω as well. The surface resistivity is determined using the following equation:

$$R_s = \frac{\pi}{ln\,2} R \tag{1}$$

The value of R is obtained using the digital multimeter connected to four aligned probes and equally spaced of 1 mm. In particular, a current (I) is driven through the outer probes and the generated voltage potential (V) is measured through the inner ones. A representative scheme is shown in Fig. 6. The use of this configuration allows the elimination of the parasitic resistances that usually affects the results of two probes setup. Knowing the thickness (t) is then possible to calculate the resistivity (ρ) and so the conductivity (σ):

$$\rho = R_s \cdot t = [\Omega \cdot m] \tag{2}$$

$$\sigma = 1/\rho = [S] \tag{3}$$

Wettability tests were conducted with a custom setup consisting of a 10 µL micropipette to obtain a water droplet of controlled volume, a Supereyes B008 HD Digital Microscope for image acquisition and a stage with fine-movement control to ensure the right positioning of the sample with respect to the camera. The drawing of the tangent lines, of the baselines and the angle measurements were conducted using the software "Image J".

Three point bending tests were conducted using an Instron 3369 Universal Testing Machine with a 1 kN load-cell. The standard procedure ISO 14125, adapted for thin samples, was followed, applying a strain rate of 10^{-3} s^{-1}. These tests were conducted for two different purposes: calculation of the Flexural Modulus and evaluation of the adhesion between the RGO Film and the CFRP laminate. Three different samples were tested, each having at least five specimens: reference CFRP laminate (B), multifunctional RGO/CFRP laminate with the RGO Film on top (MT), and multifunctional RGO/CFRP laminate with the RGO Film on bottom (MB). In Table 1 sample characteristics are reported while a representative scheme is shown in Fig. 2.

Table 1. Summary of samples configuration and size for three point bending tests.

Sample	Unit	B	MT	MB
Length	[mm]	40	40	40
Width	[mm]	15	15	15
Span	[mm]	28	30	30
Thickness	[mm]	0.68	0.72	0.78

Fig. 2. Scheme of the three different samples for three point bending tests.

During the bending tests, live resistance measurements in four point probe configuration were recorded using an Agilent 34401 Digital Multimeter. The aim was to study the live strain sensing function of the coating. The connections were made installing two silver/epoxy electrodes on the RGO film and placing two leads per electrode. A representative scheme and the wired sample are shown in Fig. 3.
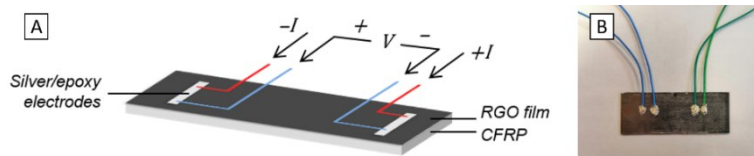

Fig. 3. (A) Electrodes configuration scheme of live resistance measurements
during the bending tests and (B) wired sample.

The thermal properties where examined performing DC-biased Thermography with a Velleman LABPS1503 DC power supply and a CEDIP Jade 3 MWIR (3-5 µm spectral range, 320 x 250 pixel resolution, average NEDT of 20 mK) thermal radiometer for Infra-Red (IR) images. Two different tests were performed: in the first one 15 s of DC heating (1 Ampere) were instantaneously followed by 15 s of cooling by ambient air blown from fans; while in the second one the temperature of the surface was monitored during 30 s of DC heating (1 A).

3. Results and Discussion

The X-Ray diffraction pattern of the RGO film is shown in Fig. 4. It is possible to observe the presence of three main peaks at 26.5 °, 42.3 ° and 44.5 °. While the first correspond the (002) graphitic phase, the second and the third determine the longitudinal dimension of the structural elements, respectively corresponding to the indexes (004) and (006) [23]. With the application of Bragg's law

$$d = \lambda/2 \sin \theta \qquad (4)$$

where λ is the radiation wavelength and θ is the reflection angle of the (002) phase, the interplanar distance d can be calculated [24]. The resulting value, d = 3.361 Å, is only slightly higher than the typical value of graphite, d = 3.338 Å, confirming that a very high degree of reduction of the Graphene Oxide has been achieved during the manufacturing of the film [25].
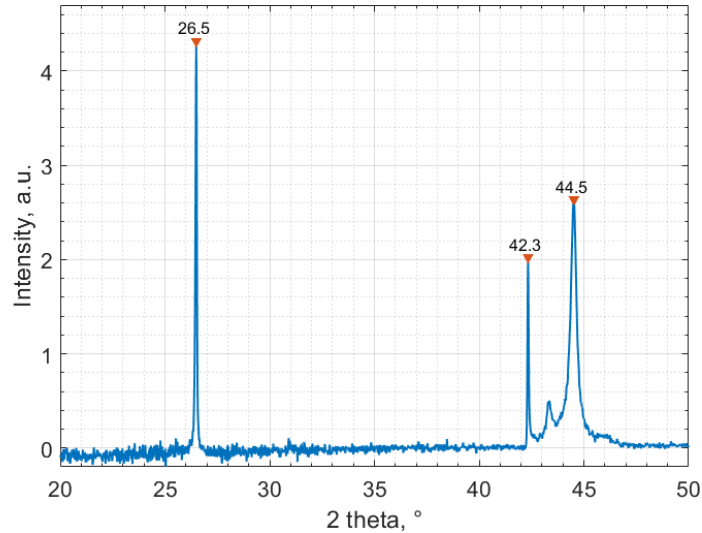

Fig. 4. XRD Pattern of the RGO film.

The Raman spectra of carbons materials are characterized by two main bands, the G and D, and by the secondary 2D band. The G band, usually lying at ≈1560 cm^{-1}, is relative to primary in-plane vibrations mode between pairs of sp^2 atoms in both rings and chains, the D band, ≈1360 cm^{-1}, arises from the breathing modes of sp^2 atoms in rings, and the 2D band, ≈2710 cm^{-1}, is a second order overtone of the D band. The RGO film presents the G and 2D bands, with the peaks at 1582 and ≈2700 cm^{-1}, but not the D one (Fig. 5). Moreover, the 2D consists of two components having peaks at 2677 and 2680 cm^{-1}. The last feature is an evidence that the film structure is based on the stacking of more than five Graphene layers, allowing a comparison with bulk graphite [26].
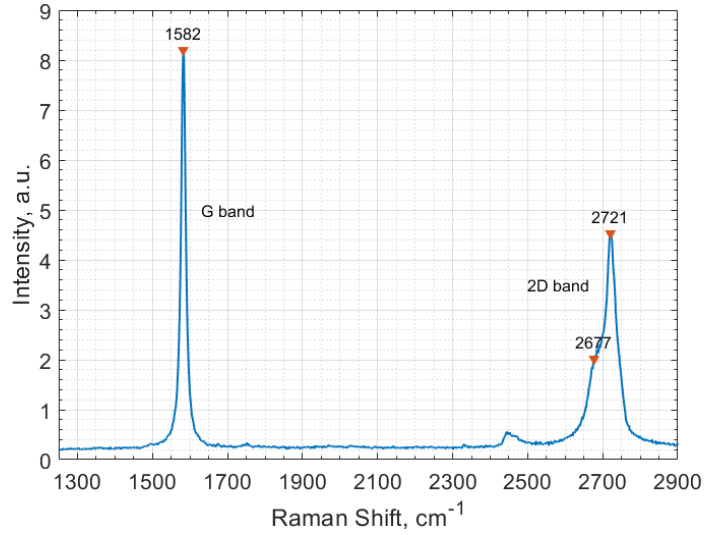
Fig. 5. Raman spectrum of the RGO film.

Table 2 summarises the results of the Surface Resistivity measurements on the coated side of the multifunctional composite and on the uncoated reference sample. The extremely high conductivity of the RGO film is not affected by the laminate manufacturing process and allows an increase of 9 orders of magnitude of the electrical conductivity of the coated laminate with respect to the reference.

Table 2. Electrical conductivity measurements of the multifunctional composite on the coated sample (RGO) and on the reference one (CFRP).

Sample	Thickness, t	Sheet Resistance, R_s	Conductivity, σ
Unit	[m]	[Ω sq^{-1}]	[S]
Coated	$40 \cdot 10^{-6}$	$4.08 \cdot 10^{-2}$	$6.13 \cdot 10^{5}$
Reference	$200 \cdot 10^{-6}$	$1.59 \cdot 10^{-7}$	$3.15 \cdot 10^{-4}$

In order to evaluate the wettability, measurements of the static contact angle between both the uncoated and coated multifunctional laminate and a water droplet were performed, as shown in Fig. 7. The contact angle values, reported in Table 3, are equal to 95 ° and 60 °, respectively for the coated and uncoated side. This demonstrates that, because of the coating presence, the laminate can show a hydrophobic behaviour, due to the angle larger than 90 °, while the uncoated side is hydrophilic, showing an angle smaller than 90 ° [27].
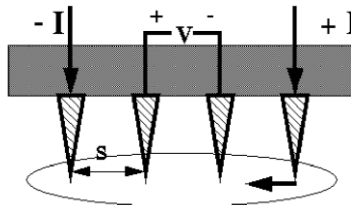

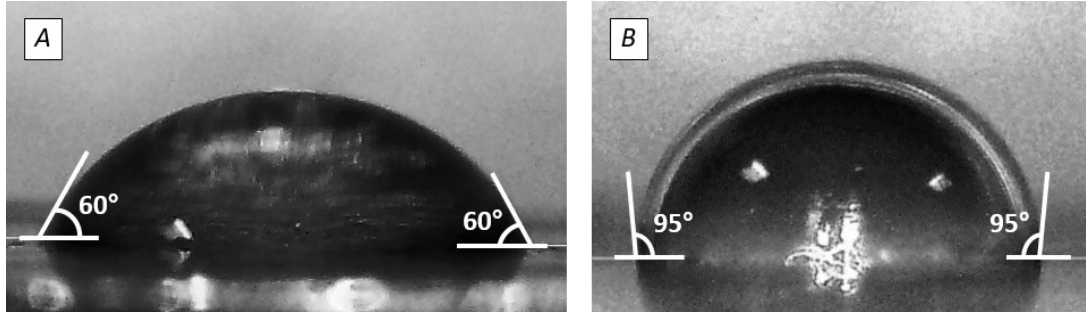Fig. 6. Scheme of four point probes measurements.

Fig. 7. Pictures of the water droplet on the CFRP (A) and RGO (A) sides of the laminate, with representative angles.

Table 3. Average contact angle of the water droplet on the laminate surface.

Sample	Contact Angle	Standard Deviation
Coated	95°	3°
Uncoated	60°	1°

Three point bending tests results are reported in Table 4. It is possible to observe a Flexural Modulus reduction from 111.1 GPa of the reference, sample B, to 106.3 GPa and 100.8 GPa of the samples MB and MT, respectively. In the first case, it is comparable with the film to sample thickness ratio: –4.3 % decrease of flexural modulus with 5.5 % of film/sample ratio. In the second case, the loss of mechanical properties is slightly more important: –9.3 % decrease of flexural modulus with 5.5 % of film/sample ratio. These results have highlighted a detrimental effect of the RGO film on CFRP laminates flexural properties: this is, in the case of the MB sample, proportional with the increase in thickness lead by the application of the coating and unexpectedly more than proportional in the case of the MT sample. Even if the latter could still be attributable to measurement errors, more mechanical tests are required to better understand this response of the structure.

Table 4. Summary of the experimental results of three point bending tests.

Sample	Flexural Modulus			Thickness		
	Value	Standard Deviation	To Reference Variation	Overall sample	Film	Film/Sample Ratio
Unit	[GPa]	[GPa]	[%]	[mm]	[mm]	[%]
B	111.1	1.7	-	0.68	-	-
MB	106.3	4.3	– 4.3	0.72	0.04	5.5
MT	100.8	3.4	– 9.2	0.72	0.04	5.5

Pictures shown in Fig. 8 display the multifunctional samples with the coating both on top (MT) and on bottom (MB) in three different instants of time: at the start of the test, an instant before failure and an instant after failure. Despite the high bending before the failure, when subjected to both tensile and compressive stress, the RGO film maintains full adhesion with the CFRP laminate and detachment is observed only after the failure of the main CFRP structure. Therefore, the adhesion between the coating and the composite laminate can be indirectly considered acceptable.
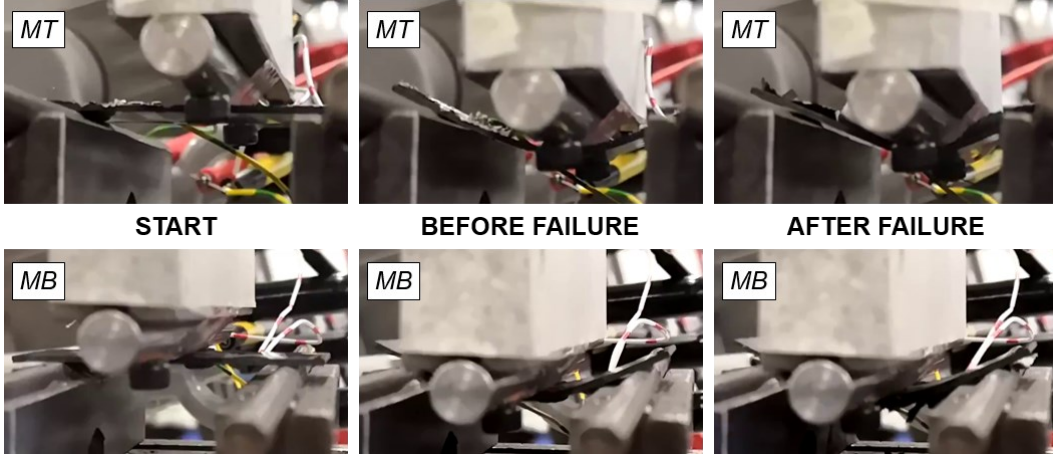
Fig. 8. Pictures of the samples MT and MB during the bending tests.

The live resistance variation measurements during the bending tests, shown in Fig. 9, produced reliable results only for the MB sample and only after a Strain Threshold of 0.010. After that value, a linear relationship between the Normalized Resistance Variation ($\Delta R\ R_0^{-1}$) and the Strain is found. The working principle of the strain-sensing feature of the coating consist in a direct relationship between the conductive film deformation and its resistance, obeying to the following equation:

$$R = \rho \cdot L/_A \qquad (5)$$

where L is the length and A is the cross-sectional area of the conductor. The reason why a strain threshold value is required could be explained considering an initial "corrugated state" of the coating that need a certain stretching of the substrate, the CFRP laminate, before starting to be actually tensioned. This would explain also the impossibility to find reliable results for the MT sample, where the coating is placed on the compressed side: in that case, during the tests, the RGO film would only change its "corrugated state" without variation of length or cross-sectional area and so of resistance. A representative scheme of this behaviour is shown in Fig. 10.
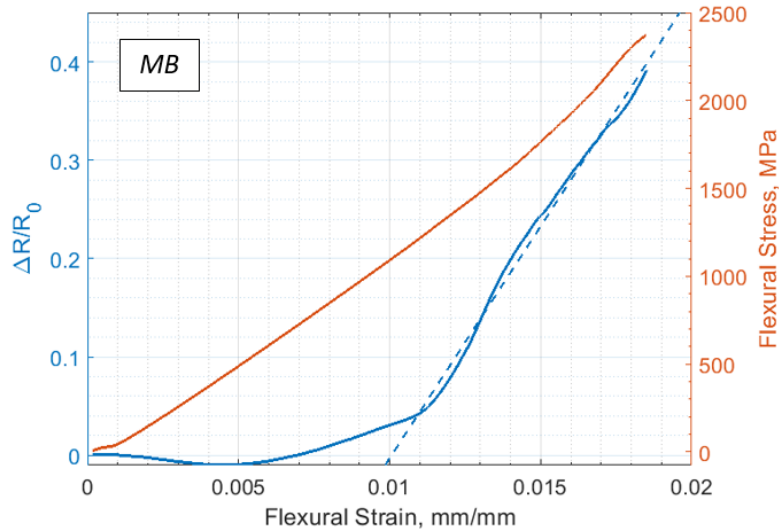

Fig. 9. Plots of the Normalized Resistance Variation ($\Delta R\ R_0^{-1}$) and Stress versus strain in MB sample. The blue dashed line is the linear fit in a strain range between 0.010 and 0.018.
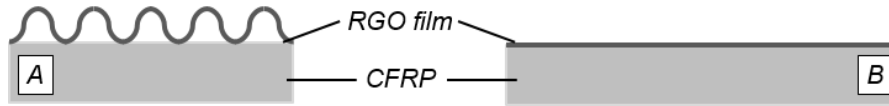
Fig. 10. Representative scheme of the initial "corrugated" state (A) and tensioned state after the strain threshold (B) of the RGO Film.

Images from the first thermographic tests are reported in **Error! Reference source not found.**. It is possible to observe how the heating in multifunctional specimens is more uniform and controlled if compared with the reference ones. In addition, the coating allows a quicker recovery of the initial condition during the cooling phase. **Error! Reference source not found.** shows that, during the 30 s of DC heating, the temperature increases linearly from 23.4 °C (Ambient Temperature) to 31.9 °C.
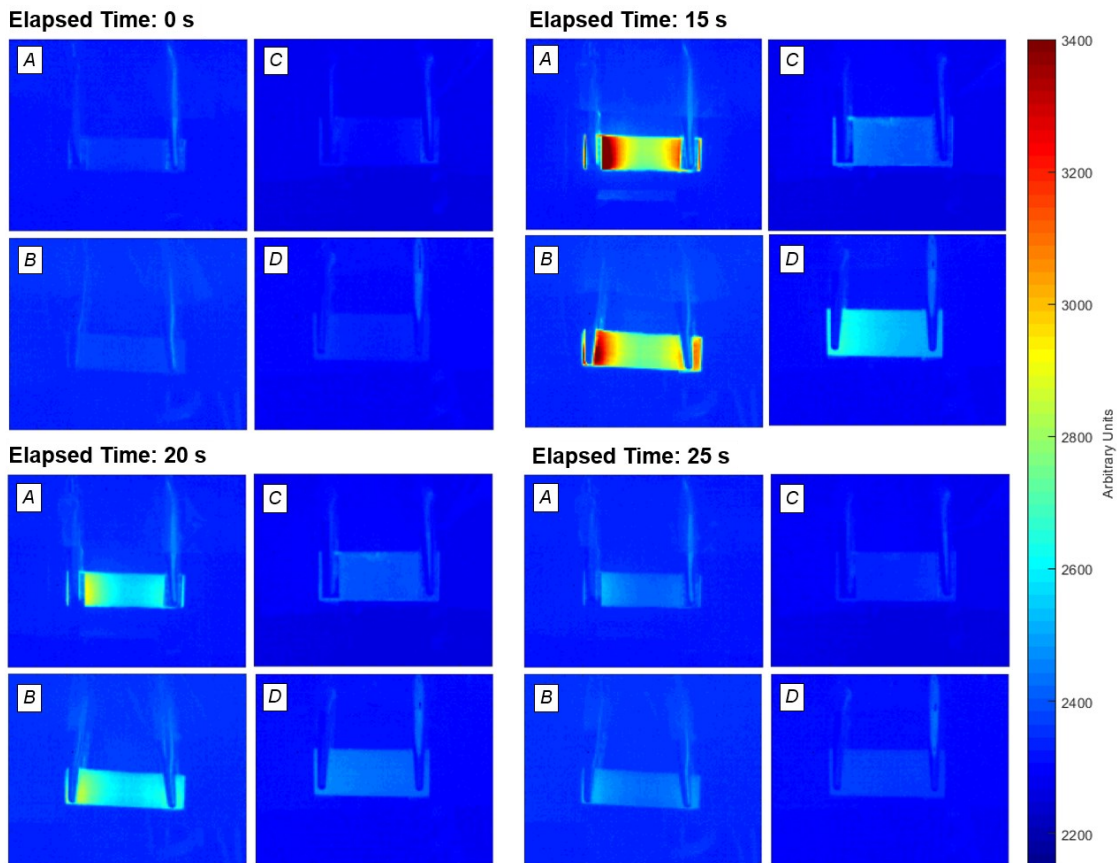

Fig. 11. IR Images of Reference CFRP Front (A), Reference CFRP Back (B), RGO/CFRP Front (coated side) (C), RGO/CFRP Back (uncoated side) (D) during the first thermography test.
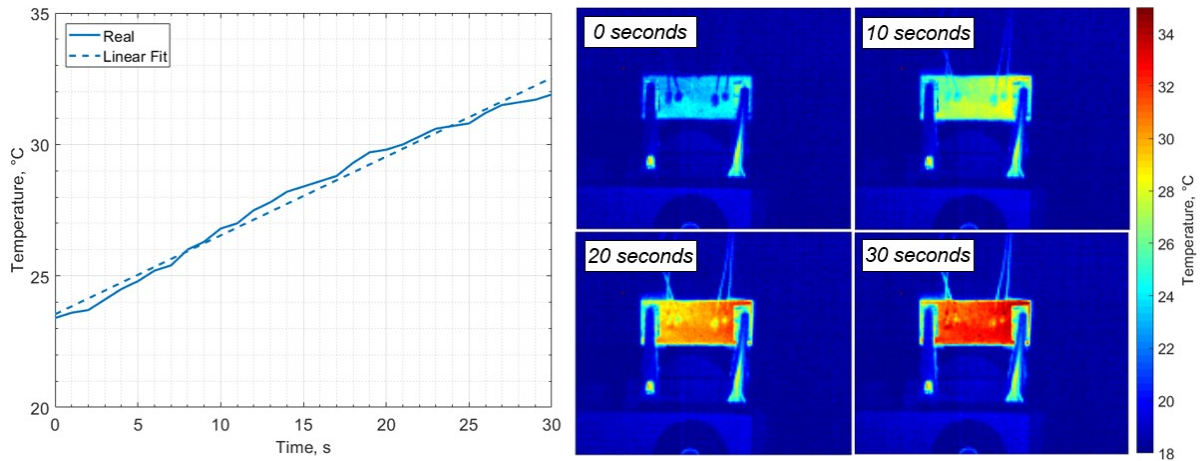
Fig. 12. Linear Fit of the Temperature increase during the 30 s of DC heating (left) and relative IR Images (right) of RGO/CFRP Front (coated side).

4. Conclusions and Future Works

In summary, a preliminary evaluation of the use of an RGO Film as a multifunctional coating of CRFPs was investigated. Chemical and physical characterisation of the RGO Film structure showed that the film manufacturing process determined a restacking of the graphene layers.

Surface properties study revealed an increase of the electrical conductivity of 9 order of magnitudes, from $3.15 \cdot 10^{-4}$ S of the uncoated side to $6.13 \cdot 10^{5}$ S of the coated one, and that a hydrophobic behaviour was successfully introduced due to the coating, verified with the measurement of a 95 ° contact angle between a water droplet and the coated surface.

Mechanical tests, consisting in three point bending, demonstrated instead a detriment of the mechanical performance, comparable with the thickness increase of the structure after the application of the coating. The same tests proved a good adhesion between the RGO Film and the CFRP laminate, indirectly evaluated analysing the failure of the specimens during the bending. In addition, for the sample having the coating on the tensioned side and only after a Strain Threshold value, a linear relationship between the Normalized Resistance Variation and the Flexural Strain was found.

Finally, the DC-biased thermography delineated that the coating allows a linear and uniform heating of the surface.

The obtained results provide motivation to continue the development and study of RGO based multifunctional coating for polymeric composite. The mechanism behind the existing relationship between the resistance variation and the strain will be evaluated, more mechanical tests will be conducted to better evaluate the influence of the RGO Film on the mechanical properties and the application of the DC-biased thermography for Damage Localisation purposes will be considered.

Acknowledgements

References

[1]   Hirsch, A., 2010. The era of carbon allotropes. Nature Materials, 9 (11), pp. 868-871.

[2]   Kroto, H.W., et al., 1985. C60: Buckminsterfullerene. Nature, 318 (6042), pp. 162-163.

[3]   Iijima, S., 1991. Helical microtubules of graphitic carbon. Nature, 354 (6348), pp. 56-58.

[4]   Novoselov, K.S., et al., 2004. Electric Field Effect in Atomically Thin Carbon Films. Science, 306 (5696), pp. 666.

[5]   Lee, C., et al., 2008. Measurement of the Elastic Properties and Intrinsic Strength of Monolayer Graphene. Science, 321 (5887), pp. 385.

[6]   Balandin, A.A., 2011. Thermal properties of graphene and nanostructured carbon materials. Nature Materials, 10, pp. 569.

[7]   Xin, G., et al., 2015. Highly thermally conductive and mechanically strong graphene fibers. Science, 349 (6252), pp. 1083.

[8]   Leenaerts, O., B. Partoens, and F.M. Peeters, 2009. Water on graphene: Hydrophobicity and dipole moment using density functional theory. Physical Review B, 79 (23), pp. 235440.

[9]   Dreyer, D.R., et al., 2010. The chemistry of graphene oxide. Chemical Society Reviews, 39 (1), pp. 228-240.

[10]   Zhu, Y., et al., 2010. Graphene and Graphene Oxide: Synthesis, Properties, and Applications. Advanced Materials, 22 (35), pp. 3906-3924.

[11]   Chandra, V., et al., 2010. Water-Dispersible Magnetite-Reduced Graphene Oxide Composites for Arsenic Removal. ACS Nano, 4 (7), pp. 3979-3986.

[12]   Chen, D., H. Feng, and J. Li, 2012. Graphene Oxide: Preparation, Functionalization, and Electrochemical Applications. Chemical Reviews, 112 (11), pp. 6027-6053.

[13]   Kim, H., A.A. Abdala, and C.W. Macosko, 2010. Graphene/Polymer Nanocomposites. Macromolecules, 43 (16), pp. 6515-6530.

[14]   Shahil, K.M.F. and A.A. Balandin, 2012. Thermal properties of graphene and multilayer graphene: Applications in thermal interface materials. Solid State Communications, 152 (15), pp. 1331-1340.

[15]   Kim, K., et al., 2008. Electric Property Evolution of Structurally Defected Multilayer Graphene. Nano Letters, 8 (10), pp. 3092-3096.

[16]   Soutis, C., 2005. Carbon fiber reinforced plastics in aircraft construction. Materials Science and Engineering: A, 412 (1), pp. 171-176.

[17]   Bakis, C.E., et al., 2002. Fiber-reinforced polymer composites for construction - State-of-the-art review. Journal of Composites for Construction, 6 (2), pp. 73-87.

[18]   Harris, C.E., J.H.S. Jr., and M.J. Shuart, 2002. Design and Manufacturing of Aerospace Composite Structures, State-of-the-Art Assessment. Journal of Aircraft, 39 (4), pp. 545-560.

[19]   Rizzo, F., F. Pinto, and M. Meo, 2019. Development of multifunctional hybrid metal/carbon composite structures. Composite Structures, 222, pp. 110907.

[20]   Matsuzaki, R., M. Melnykowycz, and A. Todoroki, 2009. Antenna/sensor multifunctional composites for the wireless detection of damage. Composites Science and Technology, 69 (15), pp. 2507-2513.

[21]   Wang, H., et al., 2018. Through-thickness thermal conductivity enhancement of graphite film/epoxy composite via short duration acidizing modification. Applied Surface Science, 442, pp. 170-177.

[22]   Sairajan, K.K., G.S. Aglietti, and K.M. Mani, 2016. A review of multifunctional structure technology for aerospace applications. Acta Astronautica, 120, pp. 30-42.

[23]   Popova, A.N., 2017. Crystallographic analysis of graphite by X-Ray diffraction. Coke and Chemistry, 60 (9), pp. 361-365.

[24]   Bragg William, H. and L. Bragg William, 1913. The reflection of X-rays by crystals. Proceedings of the Royal Society of London. Series A, Containing Papers of a Mathematical and Physical Character, 88 (605), pp. 428-438.

[25]   Pei, S., et al., 2010. Direct reduction of graphene oxide films into highly conductive and flexible graphene films by hydrohalic acids. Carbon, 48 (15), pp. 4466-4474.

[26]   Ferrari, A.C., 2007. Raman spectroscopy of graphene and graphite: Disorder, electron–phonon coupling, doping and nonadiabatic effects. Solid State Communications, 143 (1), pp. 47-57.

[27]   Wenzel, R.N., 1936. Resistance of solid surfaces to wetting by water. Industrial and Engineering Chemistry, 28 (8), pp. 988-994.